Morphology and Transverse Stiffness of *Drosophila* Myofibrils Measured by Atomic Force Microscopy

Lori R. Nyland and David W. Maughan
Department of Molecular Physiology and Biophysics, University of Vermont, Burlington, Vermont 05405, USA

ABSTRACT Atomic force microscopy was used to investigate the surface morphology and transverse stiffness of myofibrils from *Drosophila* indirect flight muscle exposed to different physiologic solutions. I- and A-bands were clearly observed, and thick filaments were resolved along the periphery of the myofibril. Interfilament spacings correlated well with estimates from previous x-ray diffraction studies. Transverse stiffness was measured by using a blunt tip to indent a small section of the myofibrillar surface in the region of myofilament overlap. At 10 nm indention, the effective transverse stiffness ($K_\perp$) of myofibrils in rigor solution (ATP-free, pCa 4.5) was 10.3 ± 5.0 pN nm^{-1} (mean ± SEM, $n = 8$); in activating solution (pCa 4.5), 5.9 ± 3.1 pN nm^{-1}; and in relaxing solution (pCa 8), 4.4 ± 2.0 pN nm^{-1}. The apparent transverse Young's modulus ($E_\perp$) was 94 ± 41 kPa in the rigor state and 40 ± 17 kPa in the relaxed state. The value of $E_\perp$ for calcium-activated myofibrils (55 ± 29 kPa) was approximately a tenth that of Young's modulus in the longitudinal direction, a difference that at least partly reflects the transverse flexibility of the myosin molecule.

INTRODUCTION

Striated muscle fibers consist of numerous myofibrils, each of which is a highly ordered array of interdigitating thick filaments (containing myosin II molecules) and thin filaments (containing actin molecules). Fueled by MgATP hydrolysis, contractile forces are produced by cyclic interactions of myosin with actin (Huxley, 1957; Huxley, 1969)

The actomyosin cross-bridges have components of elasticity and force that are directed both longitudinally and transversely with respect to the filament axes (Schoenberg, 1980a,b). Although the longitudinal component of elasticity is usually studied by analyzing force responses to length perturbations at the ends of the muscle fibers, other techniques must be used to study the transverse component. The usual approach to measuring transverse elasticity is to compress a demembranated muscle fiber using large colloids of known osmotic pressure, and then to divide the osmotic pressure by the change in fiber width or myofilament lattice spacing (see Millman, 1998, for review). Recently, however, a method based on atomic force microscopy (Binnig, 1986) has been used to estimate myofilament lattice elasticity, or stiffness, by measuring the force required to indent the surface of a myofibril (Nyland et al., 1997; Yasuike et al., 1998; Yoshikawa et al., 1999). Because the indentations are carried out on intact myofibrils or myofibrillar fragments, elastic contributions from structures other than the myofilament lattice are eliminated, thereby simplifying certain aspects of the structural analysis. The localization of stiffness measurements to uniform regions of the sarcomere (such as the A-band, where thick and thin filaments overlap) further simplifies the analysis.

In this study, we examined the morphology and transverse stiffness of myofibrils from insect indirect flight muscle. *Drosophila* was chosen because of its potential usefulness in evaluating changes in morphology and viscoelasticity produced by genetic alterations of myofibrillar structures (Sparrow et al., 1991; Maughan and Vigoreaux, 1999).

MATERIALS AND METHODS

Sample preparation

Dorsal longitudinal flight muscle fibers were dissected from the thoraces of wild type (Canton S) *Drosophila* at 4°C in relaxing solution containing the detergent Triton X-100 (0.5% w/v). The relaxing solution (pCa 8) contained (in mM) 5.50 Na_2ATP, 6.12 $MgCl_2$, 0.11 $CaCl_2$, 122.3 K methanesulfonate (KMS), 5 EGTA, 20 *N*-bis [2-hydroxyethyl]-2-aminoethanesulfanic acid (BIS), 0.25 dithiothreitol (DTT), and 10 μg/ml leupeptin. The fibers were incubated in the Triton-containing relaxing solution for 1–2 h, during which the cellular membranes, including those of the mitochondria and sarcoplasmic reticulum, were solubilized (i.e., the fibers were "skinned"). The skinned fibers were washed with detergent-free relaxing solution and stored at −20°C in relaxing solution containing 50% (w/v) glycerol. Upon use, 1–2 fibers were divided length-wise into bundles of myofibrils, and washed with a rigor solution (pCa 4.5) containing (in mM) 4.96 $CaCl_2$, 122 KMS, 5 EGTA, 20 BIS, 0.25 DTT, and 10 μg/ml leupeptin. Activating solution (pCa 4.5), used later in the experiments, contained (in mM) 5.50 Na_2ATP, 6.12 $MgCl_2$, 5.02 $CaCl_2$, 122.3 KMS, 5 EGTA, 20 BIS, 0.25 DTT, and 10 μg/ml leupeptin. Ionic strength of all solutions was 0.175 M; pH, 7.0; temperature, 22 ± 1°C.

Glass slides were used as substrates for the myofibrils. To prepare slides for adhering myofibrils by means of electrostatic interactions, slides were cleaned and incubated in 100 mM $MgCl_2$ for 2–5 days, washed, and air-dried. To prepare slides for adhering myofibrils by covalent interactions, slides were stored in a dessicator containing 1–2 ml aminopropyltriethoxysilane (Osi Specialties, Inc., Sistersville, WV) for 2–5 days. Myofibrillar bundles in rigor solution were deposited onto the treated glass slide. Centrifugation of the slide (800 rpm, 6 min) resulted in thousands of individual myofibrils being deposited on the slide's surface.

Received for publication 23 September 1999 and in final form 27 November 1999.

Address reprint requests to David W. Maughan, Department of Molecular Physiology and Biophysics, University of Vermont, Burlington, VT 05405. Tel.: 802-656-4041; Fax: 802-656-0747; E-mail: maughan@salus.uvm.edu.

© 2000 by the Biophysical Society

0006-3495/00/03/1490/08 $2.00

Imaging

Images of the myofibrils in solution were acquired with a commercial atomic force microscope (AFM). The AFM (Nanoscope IIIa, Digital Instruments, Santa Barbara, CA) was mounted on an Olympus IX-70 inverted light microscope (Olympus America, Inc., Melville, NY). The entire assembly was isolated from wind currents and room vibration by a shielded vibration isolation table (MICRO-g, Technical Manufacturing Corp., Peabody, MA). The myofibril-coated glass slide was secured to the stage of the microscope with tape. Triangular cantilevers (200 μm long; manufacturer rated spring constant, 60 pN nm^{-1}) with oxide-sharpened silicon nitride tips (radius of curvature, 10–40 nm) were used for imaging (Nanoprobe, Digital Instruments). Tips were aligned over an isolated myofibril using the inverted light microscope and its *x*-*y* stage positioners. A piezoelectric stack controlled by the AFM software lowered the tip/cantilever assembly to the myofibrillar surface. To obtain optimal image quality, "Tapping Mode" was operated at relatively slow scan frequencies (0.5–1 Hz), capturing 256 samples per line. Imaging forces were minimized by adjusting the set point.

Software provided with the AFM was used to analyze the surface profile of the captured images. To quantify filament spacing along the periphery of the myofibrillar lattice, virtual markers were placed at the center of each filament and the AFM software was used to calculate the horizontal distance between the markers.

Transverse stiffness

Transverse stiffness was measured using relatively large spherical tips of silicon nitride (MatTips, Bioforce Laboratory, Santa Barbara, CA). Spherical tips (radius of curvature, 1 μm) distributed the strain more uniformly than pointed tips. Their bluntness also prevented the tip from breaking into the myofibril, as appeared to be the case using tips whose radius of curvature was comparable to interfilament spacing. The length of the cantilever and spring constant were supplied by the manufacturer (200 μm long; 60 pN nm^{-1}). Before the stiffness measurement, myofibrils were rastered in Tapping Mode using the blunt tip. Up to 10 consecutive half-sarcomeres were scanned (scanned field, 20 μm $\times$ 20 μm). At each half-sarcomere, we zoomed in on the center of the A-band portion, and then reduced the scan size to zero. The surface was probed at 1 Hz in Force Mode, and the transverse stiffness at that location calculated from a force plot acquired using the AFM system software (Radmacher, 1997; Shroff et al., 1995).

Stiffness measurements were made in different solutions on the same set of half-sarcomeres. Solutions were exchanged in the following sequence: rigor solution, activating solution, relaxing solution, and rigor solution containing 1% (v/v) glutaraldehyde. The calcium concentration of the activating solution (pCa 4.5) was sufficient to yield maximum activation (Dickinson et al., 1997). Commercial statistical software (Systat, Evanston, IL) was used for basic statistics (means, standard errors) and for analysis of variance.

RESULTS AND DISCUSSION

Surface morphology

An AFM image of a myofibril in rigor is shown in Fig. 1. An oxide-sharpened silicon nitride tip was used to obtain the image, shown at two magnifications (*a* and *b*). Filaments that run axially along the myofibril are clearly resolved. Debris appears as random bumps along the surface. Short I-bands (thin filament region) with the protruding Z-band in the middle are clearly distinguished from the long A-bands (thick and thin filament overlap region) centered on the M-lines. Activated and relaxed myofibrils (not shown) are virtually indistinguishable from those in rigor.

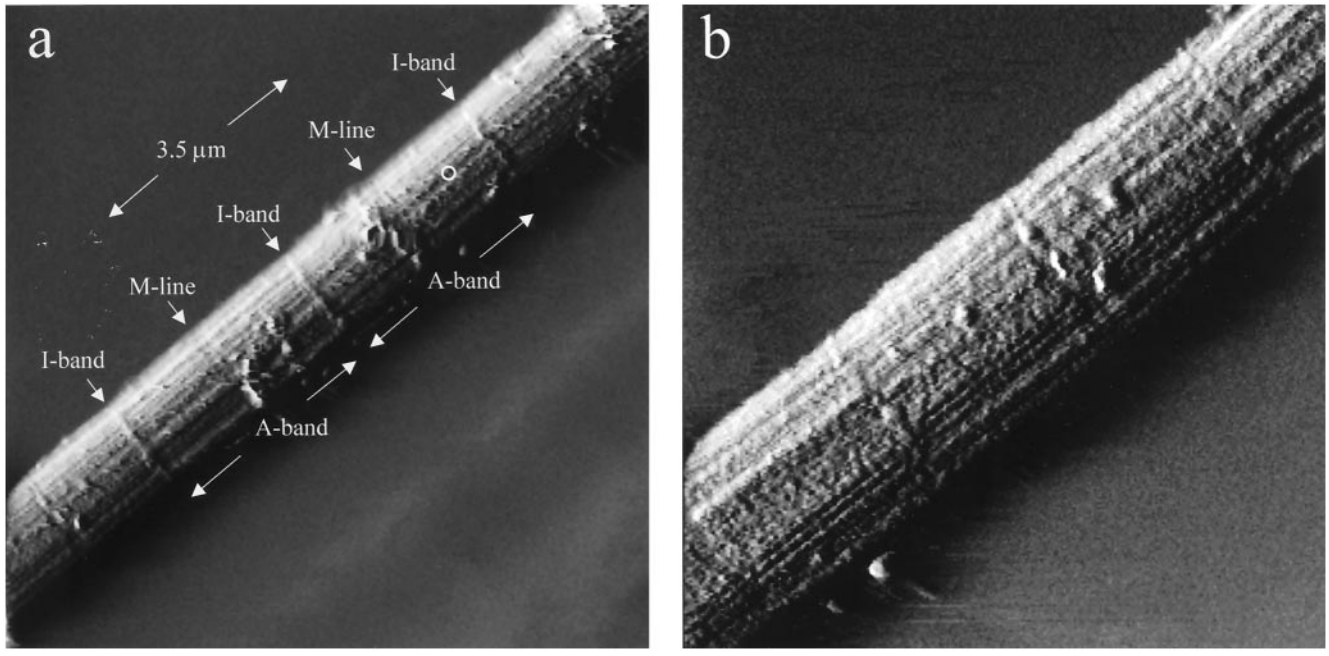

FIGURE 1 Atomic force microscopy of a *Drosophila* IFM myofibril in rigor solution. Image size: (*a*) 10 μm $\times$ 10 μm (pixel size, 39 nm); (*b*) 5 μm $\times$ 5 μm (pixel size, 19.5 nm). Sarcomere length, 3.5 μm. Labels indicate I-band, A-band, and M-line structures. The surface area contacted by the tip during the stiffness measurements is shown as a circle. Images (error mode) were acquired in Tapping Mode.

Firm attachment of myofibrils to the glass substrate was indicated by the clarity of the image, with little evidence of hysteresis or jitter with rastering. Firm attachment was also indicated by myofibrils remaining virtually isometric after switching to activating or relaxing solution (sarcomere length in rigor, 3.39 ± 0.36 μm; activated, 3.36 ± 0.33 μm; relaxed, 3.44 ± 0.22 μm). Bundles of unattached myofibrils (untreated glass) switched to activating solution slowly shortened, to a final length of about half their initial length over a period of a few minutes.

Figure 2 *a* shows a 3-dimensional close-up view of the myofibril's surface at one region of the A-band. The curvature of the myofibril is evident by the lightly shaded features near the top contrasting with the darker features nearer the sides. The filaments visible in Fig. 2 *a* probably include thick filaments but not thin filaments, because the tip's aspect ratio and radius of curvature, although small, are still too large to allow clear definition of the thinner filaments. However, the 60–70-nm periodicity of projections emanating from the thick filaments is roughly twice the 38–39-nm cross-bridge periodicity of insect flight muscle observed in electron micrographs (Taylor et al., 1993; Schmitz et al., 1994) and x-ray diffraction patterns (Reedy and Reedy, 1985; Taylor et al., 1993; Schmitz et al., 1994; Tregear et al., 1998). The appearance and the true longitudinal periodicity of myosin heads along the thick filaments is probably obscured by the comparable size of the AFM image pixel (39 nm = 10 μm/256 samples per line). Thus, the 60–70-nm spaced projections of Fig. 2 *a* are either a scanning artifact, or an unusual clumping of heads projecting from the myosin filaments.

Analysis of the surface profile (Fig. 2 *b*) reveals a variety of thick-to-thick filament spacings along the rounded periphery of the hexagonal myofilament lattice. Figure 3 illustrates the expected variation in thick filament center-to-center spacing. The four smallest and most frequently occurring spacings at the periphery are 55, 95, 146, and 198 nm, given a $d_{1,0}$ spacing of ~48 nm (Irving and Maughan,

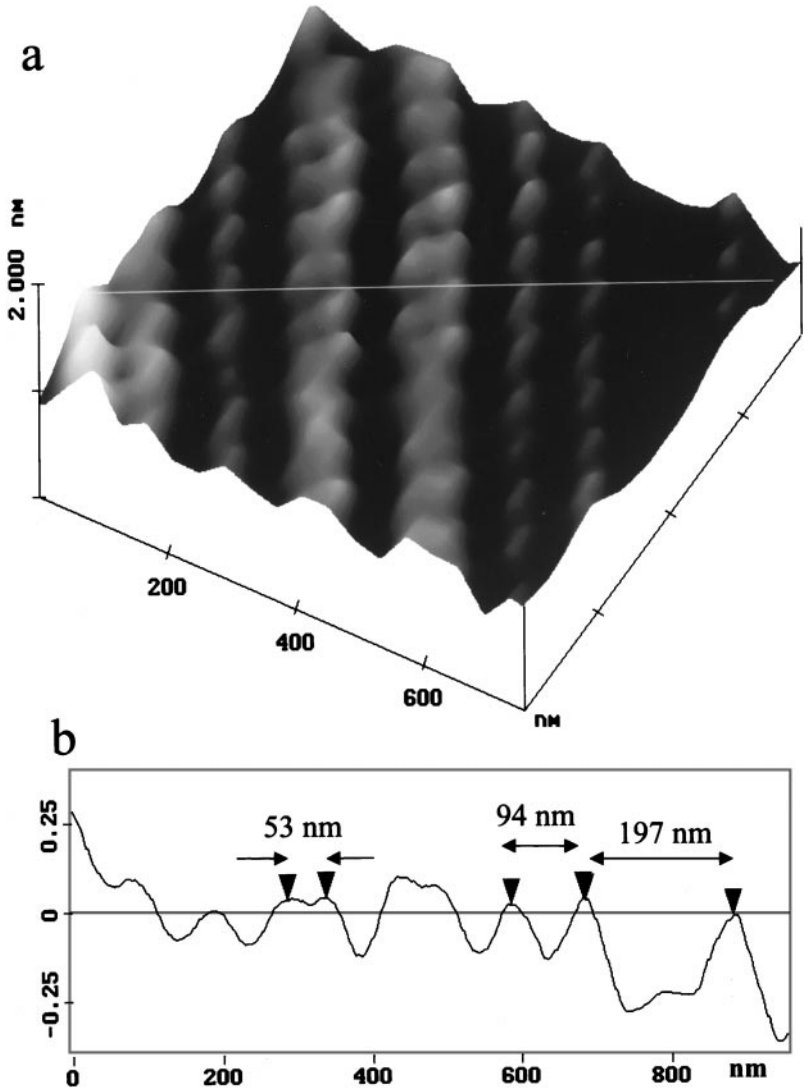

FIGURE 2 Close up view of the *Drosophila* IFM myofibrillar surface. (*a*) Error mode, 3-dimensional display, image size 750 nm × 750 nm (pixel size, 2.925 nm). The broad filaments are probably myosin-containing thick filaments, imaged singly or as doublets. The knobby appearance is most likely an AFM imaging artifact. (*b*) Section analysis surface profile, obtained at the location where the white line is drawn on *a*. Markers (*solid triangles*) locate the tops of the putative thick filaments. The horizontal distance between markers was calculated using AFM software.

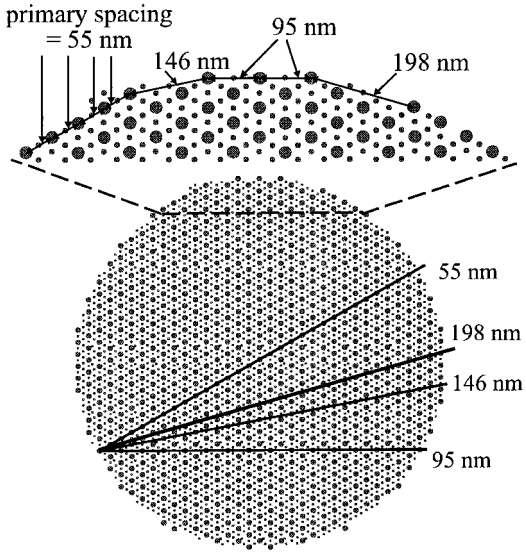

FIGURE 3 Illustration (to scale) of the hexagonal lattice in the A-band region of the *Drosophila* IFM myofibril. The lines cut through 4 planes within the lattice where the thick-to-thick filament spacing is least. Calculation of the thick-to-thick filament spacing along these planes is based on a 55-nm primary spacing at the myac layer ($2/\sqrt{3} \times d_{1,0}$, where $d_{1,0} \sim$ 48 nm: Irving and Maughan, 1999). Note diverse spacings along the periphery due to the intersection of different planes of the lattice at the surface of the myofibril.

1999). The observed center-to-center spacings (Fig. 2 *b*) are in reasonable agreement with the predicted values of Fig. 3. The distribution and values of the thick filament spacings were not noticeably different for the rigor, active, and relaxed states.

Transverse stiffness and Young's modulus

Figure 4 illustrates cantilever deflection versus piezoelectric extension, i.e., a plot of the kind used to calculate cantilever force as a function of specimen indentation. A spherical silicon nitrite tip was used and, in the case of Fig. 4 *a*, the specimen was the glass substrate or the myofibril in rigor. The point at which the blunt tip initially contacted the glass surface is easily identified, but the exact point at which the tip contacted the more compliant surface of the myofibril is not obvious. We therefore developed a method that allowed us to determine unambiguously the point at which the tip initially contacts the surface of the specimen. This point was determined by smoothing the raw cantilever deflection data (Fig. 4 *a*), and then calculating the first- (Fig. 4 *b*) and second- (Fig. 4 *c*) derivatives of the filtered cantilever deflection signal (*D*). The point at which the greatest change in *D* occurred (i.e., at the maximum d^2D/dZ^2: Fig. 4 *c*, *asterisk*) is the point at which the tip initially contacts the surface (see Fig. 4 legend for details).

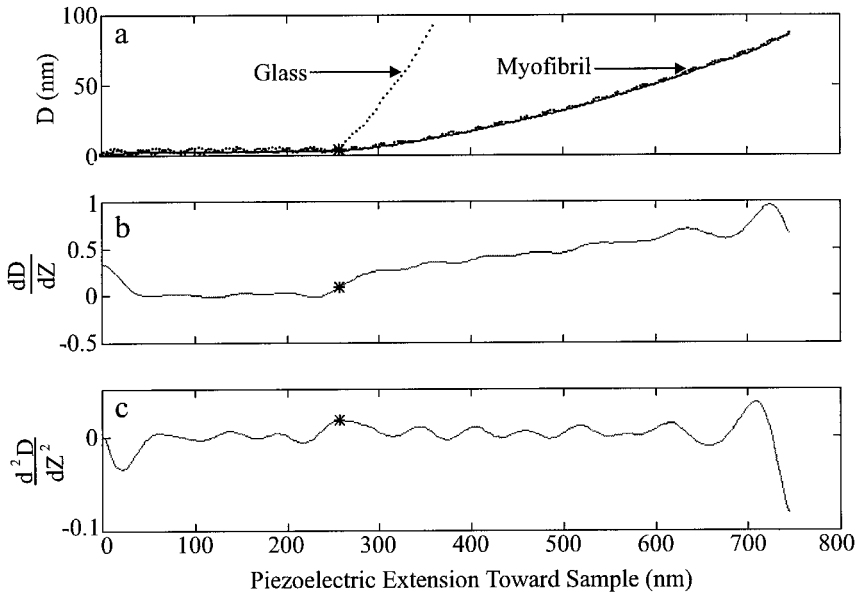

FIGURE 4 AFM force plots. (*a*) Cantilever deflection (*D*) versus piezoelectric extension (*Z*) toward sample (glass or myofibril in rigor solution). After contact with glass, cantilever deflection equals the movement of the piezoelectric. After contact with the myofibril, cantilever deflection is less than the movement of the piezoelectric due to indentation of the surface. The raw cantilever deflection data is shown as points; the solid line represents the filtered cantilever deflection signal. (*b*) Plot of the first derivative of *D* versus piezoelectric extension (*Z*) toward the sample. (*c*) Plot of the second derivative of *D* versus piezoelectric extension toward the sample. The asterisks indicate the point at which the change in d*D*/d*Z* is greatest. Only data to the right of this point were analyzed (i.e., from the point of initial contact to the 10-nm indentation of the surface. To reduce high frequency noise, a four-pole digital Butterworth filter was used and the cutoff frequency was adjusted (0.25–1.0 nm^{-1}) until the derivatives of the high frequency noise were minimized. Filter anomalies at the ends of the data file were disregarded.

Figure 5 illustrates deflection–extension (force) curves obtained at the same myofibrillar A-band location, but for 4 different ionic conditions. A force curve from glass is shown for comparison. The probability of sampling the same number of thick and thin filaments over repeated measurements was enhanced by using a blunt probe rather than a sharp one. Transverse stiffness (the slope of the deflection–extension curve) depended on solution composition. The relaxed myofibril (pCa 8) was least stiff (slope $\ll$ 1:1), calcium-activated muscle (pCa 4.5) was stiffer, and rigor muscle (no MgATP) was stiffer yet. Muscle fixed with glutaraldehyde was stiffest, reflecting extensive cross-linking of the myofibrillar proteins. Glass was not indented (slope 1:1), with cantilever deflection identical to piezoelectric extension.

The relation between indentation and applied force was nonlinear, due, at least in part, to increased area of contact of the spherical tip with the myofibril. Because the stiffness constant of the preparation (applied force divided by indentation) depends on the magnitude of the indentation, we defined an effective transverse stiffness ($K_\perp$) by evaluating the slope of the force–indentation curve as the indentation (δ) approaches zero (i.e., $\delta \rightarrow 0$):

$$K_\perp = \left.\frac{\text{applied force}}{\text{myofibrillar indentation}}\right|_{\delta\rightarrow 0} = \left.\frac{K_c D}{Z - D}\right|_{\delta\rightarrow 0}, \qquad (1)$$

where K_c is the value for cantilever stiffness (supplied by the manufacturer), D is the cantilever deflection, Z is the extension of the piezoelectric (with respect to the point at which the tip contacts the sample) and $\delta = Z - D$. $K_\perp$ was calculated by fitting a second-order polynomial to the force–indentation relations comprising each data set, and evaluating the derivatives of the polynomial fits at $\delta = 0$. Values of $K_\perp$ from 8 myofibrils are given in Fig. 6 *a*.

An apparent transverse Young's modulus ($E_\perp$) was also calculated using the Hertz equation (Yoshikawa et al., 1999), in which the cantilever tip/myofibril interaction is

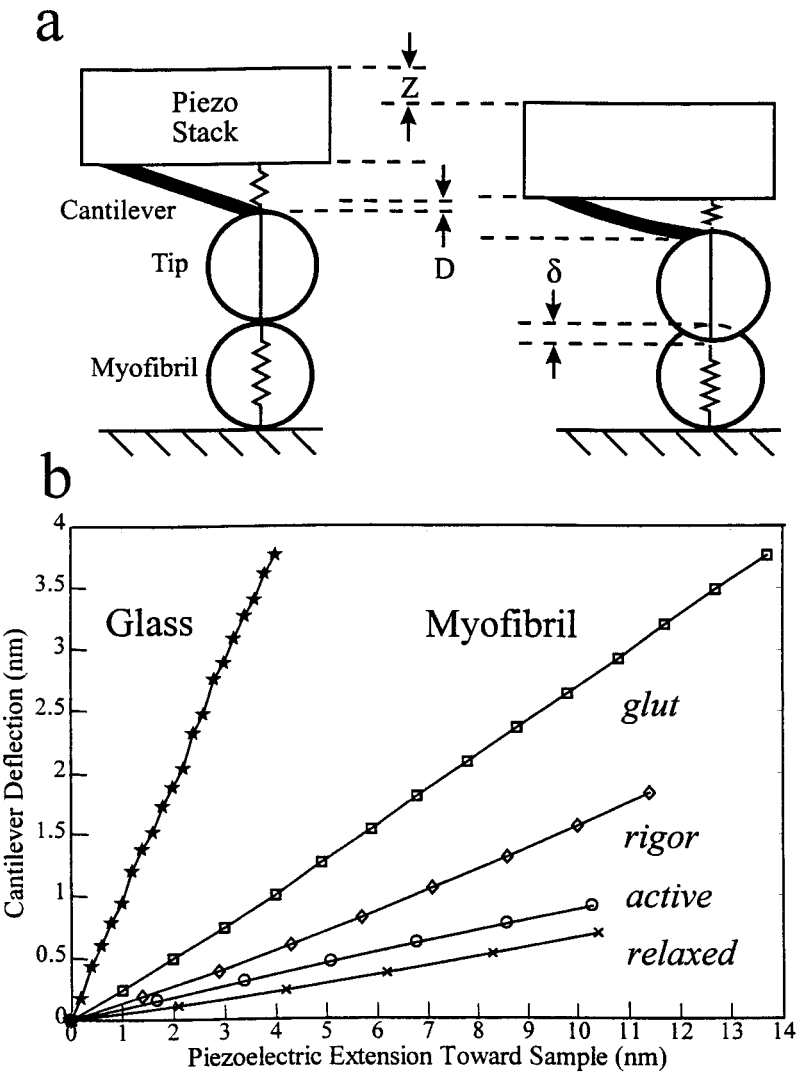

FIGURE 5 AFM tip and sample interaction. (*a*) Schematic of preparation, with variables of the force plot and Eqs. 1 and 2 defined. *Z*, piezoelectric extension; *D*, cantilever deflection; δ, indentation of the myofibril surface ($\delta = Z - D$: Eq. 2). (*b*) Representative force curves showing 10-nm indentation at the same A-band location on a myofibril in rigor, relaxed, active, and glutaraldehyde-fixed states. The stiffness of the myofibril is considerably less than that of glass (where $\Delta D/\Delta Z = 1$). Data from the force curves are used to calculate $K_\perp$ and $E_\perp$ according to Eqs. 1 and 2.

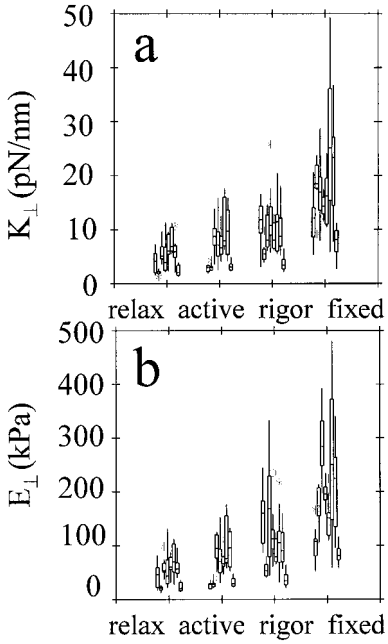

FIGURE 6 Summary of results from eight myofibrils. (*a*) Effective transverse stiffness ($K_\perp$). (*b*) Apparent transverse Young's modulus ($E_\perp$). Averages and standard deviations given for individual experiments are shown as averages (*open symbols*) and standard deviations (*error bars*). $K_\perp$ was calculated according to Eq. 1 using linear regression applied to force plots. $E_\perp$ was calculated according to Eq. 2 using nonlinear regression applied to force-indentation curves.

approximated as normal contact between an infinitely hard sphere and a compliant cylinder of uniform composition (Roark, 1965),

$$E_\perp = \lambda^{3/2}\frac{3K_cD(1-\nu^2)}{8R^{1/2}\delta^{3/2}}, \quad (2)$$

where K_c, D, and δ are defined as above, R is the radius of curvature of the sphere ($R \gg \delta$), ν is Poisson's ratio, and λ is a geometrical constant. We let $\nu = 0.5$ (assuming no volume change) and $\lambda = 1.94$ (Roark, 1965). $K_\perp$ and $E_\perp$ are effective or apparent moduli because Eqs. 1 and 2 do not take into account the anisotropy of the myofibril and any longitudinally directed stress components in the highly organized myofilament lattice. Values of $E_\perp$ for the same set of 8 myofibrils are given in Fig. 6 *b*.

Agarose was used as a validation specimen because its Young's modulus has been measured by methods other than AFM. A layer of 1% (w/v) agarose-in-water mixture in a petri dish was probed at 10 different locations, and the Young's modulus (E) was calculated from a version of the Hertz equation that assumes normal contact of an infinitely hard sphere with a soft planar surface (Hertz, 1881),

$$E = \frac{3K_cD(1-\nu^2)}{4R^{1/2}\delta^{3/2}}, \quad (3)$$

where K_c, D, R, δ, and ν are defined as above. The value of E obtained was 56 ± 25 kPa for 100-nm indentation, in reasonable accord with the Young's modulus of ~50 kPa for 1% agarose reported by Bonn et al. (1998).

Table 1 summarizes the myofibrillar results. First, consider the values of effective transverse stiffness ($K_\perp$). Ca^{2+}-activated (pCa 4.5) myofibrils were roughly 1.4× stiffer than relaxed (pCa 8) myofibrils, but only about 0.6× as stiff as myofibrils in rigor (no MgATP). Analysis of variance indicated significant differences ($p < 0.05$) in values between solutions, even though values between fibers varied appreciably. The simplest interpretation of these differences is that Ca^{2+} activation or MgATP depletion causes myosin heads to bind to actin, and that the number of heads bound in Ca^{2+}-activated myofibrils is less than that in rigor. The stiffness of the myofibril in glutaraldehyde was roughly 2× that of rigor stiffness, indicative of more extensive cross-linking.

Next, consider the apparent transverse Young's moduli ($E_\perp$). The values listed in Table 1 can be compared to those obtained from rabbit skeletal muscle myofibrils using a similar AFM indentation method (Yoshikawa et al., 1999), and from frog skeletal muscle skinned fibers using a more conventional osmotic compression method (Umazume and Kasuga, 1984). For the resting condition, $E_\perp$ of IFM (39.8 ± 17.7 kPa: Table 1) was ~4 times the values obtained from rabbit psoas muscle myofibrils (11.5 ± 3.5 kPa: Yoshikawa et al., 1999) and frog semitendinosus muscle skinned fibers (15.8 ± 4.8 kPa: Umazume and Kasuga, 1984)). The greater transverse stiffness of *Drosophila* IFM probably reflects the greater number of interfilament links (composed of unique proteins or unique extensions of conserved proteins) compared to vertebrate skeletal muscle (Maughan and Vigoreaux, 1999). For the rigor condition,

TABLE 1 Summary of Transverse Stiffness Measurements

	Relaxed		Active		Rigor		2% Glutaraldehyde	
	Mean	S.E.M.	Mean	S.E.M.	Mean	S.E.M.	Mean	S.E.M.
$K_\perp$ (pN nm^{-1})	4.4	2.0	5.9	3.1	10.3	5.0	19.0	7.2
$E_\perp$ (kPa)	39.8	17.7	54.7	29.4	93.7	41.0	172.8	65.4

$n = 8$; $K_\perp$, effective transverse stiffness (Eq. 1); $E_\perp$, apparent transverse Young's modulus (Eq. 2).
An ANOVA test showed that values of $K_\perp$ and $E_\perp$ were significantly different ($p < 0.05$) among relaxed, active, rigor, and glutaraldehyde states, when values of one state were compared to those of another. 1 kPa = 1 kN m^{-2}.

the apparent transverse Young's modulus of IFM (93.7 ± 41.0 kPa) is comparable to that reported for rabbit myofibrils (84.0 ± 18.1 kPa: Yoshikawa et al., 1999), but about twice that for frog skinned fibers (48.2 ± 18.8 kPa: Umazume and Kasuga, 1984)).

Returning to the values for the apparent transverse Young's modulus (Fig. 6 *b*), $E_\perp$ of Ca^{2+}-activated IFM myofibrils (54.7 kN m^{-2}: Table 1) is approximately a tenth of the longitudinal stiffness of IFM skinned fibers subjected to very small length perturbations at very low frequencies. For sinusoidal perturbations of <4 nm/half sarcomere at 0.5 Hz, the elastic modulus is ~540 kN m^{-2}: Fig 4 of Dickinson et al., 1997). However, it is important to note that, in the case of dynamic stiffness measurements, myofibrils are stretch-activated. Thus, the elastic modulus reflects cross-bridges formed during stretch-activation in addition to those formed during calcium-priming (Tregear et al., 1998). Assuming that the number of stretch-activated cross-bridges represents ~⅓–½ of the number formed during calcium-priming (Tregear et al., 1998), our present results suggest that the transverse stiffness of the cross-bridge is 13–15% of the longitudinal stiffness. The relatively low stiffness may reflect a greater flexibility of the myosin molecule in the radial direction due to proline residues at so-called hinge points (Fig. 7 *a*, after Huxley, 1969). A similar conclusion is reached if rigor stiffnesses in the transverse and longitudinal directions are compared (93.7 kN m^{-2} versus ~940 kN m^{-2}: Fig 4 of Dickinson et al., 1997). The value of the transverse Young's modulus for rabbit psoas myofibrils in rigor (~84 kN m^{-2}: Yoshikawa et al., 1999) is also considerably less than the corresponding longitudinal Young's modulus (250 ± 10 kN m^{-2}: Tawada, 1984). The results from these indirect comparisons, however, contrast with that of a more direct comparison of radial and axial stiffness in rabbit psoas muscle using osmotic compression and x-ray diffraction (Brenner and Yu, 1991). In that study, Brenner and Yu showed that radial stiffness (defined as radial force divided by lattice shrinkage) of Ca^{2+}-activated skinned fibers was similar in magnitude to the axial stiffness (defined as axial force divided by sarcomere extension).

A simple parallel spring model of the myofibrillar lattice (Fig. 7 *b*) allowed us to calculate a composite crossbridge transverse stiffness (K_{xb}) representing the summed contributions of individual cross-bridges. The model assumes that $K_\perp$ is the sum of K_{xb} and the composite transverse stiffness of all other structures, the latter of which is approximated by $K_\perp$ in the relaxed state (K_{relax}). Thus, the difference in $K_\perp$ between the active or rigor state and the relaxed state represents K_{xb}, i.e.,

$$K_{xb} = K_\perp - K_{relax}. \quad (4)$$

Substituting values from Table 1 into Eq. 4, K_{xb} is 5.9 pN nm^{-1} (= 10.3–4.4 pN nm^{-1}) for the rigor state and 1.5 pN nm^{-1} (= 5.9–4.4 pN nm^{-1}) for the active state. Thus, transverse stiffness of the overlap zone of a myofibril at full calcium activation is approximately a quarter of that in rigor. This difference is somewhat less than that found in rabbit psoas skinned muscle fibers using the osmotic compression and x-ray diffraction techniques (Brenner et al., 1991), where the radial stiffness of fibers at full calcium activation was approximately one-fifth that in rigor.

In summary, we investigated the surface morphology and transverse stiffness of myofibrils from *Drosophila* indirect flight muscle exposed to relaxing, calcium-activating, rigor, and glutaraldehyde-fixation solutions. Using sharp, pyramidal-shaped AFM tips, I- and A-bands of the 3.4-μm-long sarcomeres were clearly distinguished. Thick filaments, singly or in pairs, could be resolved along the periphery of the 1.8-μm-wide myofibrils. Using spherical tips to indent the fibril's surface, measurements of transverse stiffness at the A-band under conditions of full calcium-activation yielded values that were ~40% greater than fully-relaxed myofibrils, but only ~60% that of myofibrils in rigor. The transverse stiffness of fixed myofibrils was ~2 times that of the rigor stiffness. Modeling the tip–myofibril interaction yielded values for the apparent transverse Young's moduli ($E_\perp$) of the rigor and relaxed states (94 ± 41 kPa and 40 ± 17 kPa) comparable to values reported for vertebrate skeletal muscle myofibrils and skinned fibers. The value of $E_\perp$ for calcium-activated myofibrils (55 ± 29 kPa) was considerably less (perhaps a sixth) than that of the Young's modulus in the longitudinal direction, a difference that probably reflects the transverse flexibility of the myosin molecule.

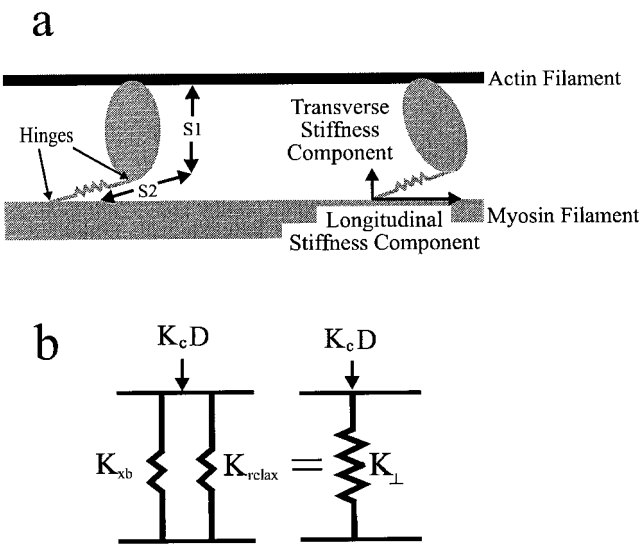

FIGURE 7 Orthogonal stiffness components. (*a*) Huxley's (1969) cross-bridge model. One hinge is located at each end of the S2 neck. Cross-bridge stiffness is composed of transverse and longitudinal components. (*b*) Spring model of the myofibrillar lattice, with apparent transverse stiffnesses of the composite elements shown. $K_\perp$ is measured stiffness, K_{relax} is the sum of the transverse stiffnesses of passive elements in the relaxed state, and K_{xb} is the sum of the transverse stiffnesses of individual cross bridges.

We thank Jon Peterson for help in analyzing the data using MATLAB. We also appreciate many helpful comments from Doug Taatjes, Jie Yang, Tony Keller, and Tony Quinn.

REFERENCES

Binnig, G. 1986. Atomic force microscopy. *Phys. Rev. Lett.* 56:930–933.

Bonn, D., H. Hellay, M. Prochnow, K Ben-Djemiaa, and J. Meunier. 1998. Delayed fracture of an inhomogenous soft solid. *Science* 280:265–267.

Brenner, B., and L. C. Yu. 1991. Characterization of radial force and radial stiffness in Ca^{2+}-activated skinned fibres of the rabbit psoas muscle. *J. Physiol.* 441:703–718.

Brenner, B., L. C. Yu, and J. M. Chalovich. 1991. Parallel inhibition of active force and relaxed fiber stiffness in skeletal muscle by caldesmon: implications for the pathway to force generation. *Proc. Natl. Acad. Sci. USA.* 88:5739–5743.

Dickinson, M. H., C. J. Hyatt, F.-O. Lehmann, J. R. Moore, M. C. Reedy, A. Simcox, R. Tohtong, J. O. Vigoreaux, H. Yamashita, and D. W. Maughan. 1997. Phosphorylation-dependent power output of transgenic flies: an integrated study. *Biophys. J.* 73:3122–3134

Hertz, H. 1881. Uber den Kontakt elastischer Korper. *J. Reine. Angew. Mathematik.* 92: 156–171.

Huxley, H. E. 1969. The mechanism of muscular contraction. *Science.* 164:1356–1366

Huxley, A. F. 1957. Muscle structure and theories of contraction. *Prog. Biophys.* 7:255–318

Irving, T., and D. Maughan. 1999. In vivo x-ray diffraction studies of indirect flight muscle from Drosophila melanogaster. *Biophys. J.* 76: A269.

Maughan, D., and J. Vigoreaux. 1999. An integrated view of insect flight muscle: genes, motor molecules, and motion. *News Physiol. Sci.* 14: 87–92

Millman, B. M. 1998. The filament lattice of striated muscle. *Physiological Rev.* 78:359–391

Nyland, L., J. Peterson, and D. Maughan. 1997. Functional and morphometric study of *Drosophila* indirect flight muscle using atomic force microscopy. *Biophys. J.* 72: A102.

Radmacher, M. 1997. Measuring the elastic properties of biological samples with the AFM. *IEEE Eng. Med. Biol.* 16:47–57.

Reedy, M. K., and M. C. Reedy. 1985. Rigor crossbridge structure in tilted single filament layers and flared-X formations from insect flight muscle. *J. Mol. Biol.* 185:145–176.

Roark, R. J. 1965. Formulas for Stress and Strain. McGraw-Hill, New York.

Schmitz, H., C. Lucaveche, M. K. Reedy, and K. A. Taylor. 1994. Oblique section 3-D reconstruction of relaxed insect flight muscle reveals the cross-bridge lattice in helical registration. *Biophys. J.* 67:1620–1633.

Schoenberg, M. 1980a. Geometrical factors influencing muscle force development. I. The effect of filament lattice spacing upon axial forces. *Biophys. J.* 30:51–67.

Schoenberg, M. 1980b. Geometrical factors influencing muscle force development. II. Radial forces. *Biophys J.* 30:69–78.

Shroff, S., D. R. Saner, and R. Lal. 1995. Dynamic micromechanical properties of cultured rat atrial myocytes measured by atomic force microscopy. *Am. J. Physiol.* 269:c286–c292.

Sparrow, J. C., D. Drummond, M. Peckham, E. Hennessey, and D. C. S. White. 1991. Protein engineering and the study of muscle contraction in *Drosophila* flight muscles. *J. Cell Sci. suppl.* 14:73–78.

Tawada, K. 1984. Stiffness of glycerinated rabbit psoas fibers in the rigor state. *Biophys. J.* 45:593–602.

Taylor, K. A., M. C. Reedy, M. K. Reedy, and R. A. Crowther. 1993. Crossbridges in the complete unit cell of rigor insect flight muscle imaged by three-dimensional reconstruction from oblique sections. *J. Mol. Biol.* 233:86–108.

Tregear, R. T, R. Edwards, T. Irving, K. Poole, M. C. Reedy, H. Schmitz, E. Towns-Andrews, and M. K. Reedy. 1998. X-ray diffraction indicates that active cross-bridges bind to actin target zones in insect flight muscle. *Biophys. J.* 74:1439–1451.

Umazume, Y., and N. Kasuga. 1984. Radial stiffness of frog skinned muscle fibers in relaxed and rigor conditions. *Biophys. J.* 45:783–788.

Yasuike, T., Y. Yoshikawa, and T. Yamada. 1998. AFM studies of the surface structures of myofibrils of rabbit skeletal muscle. *J. Mus. Res. and Cell Motil.* 19:446.

Yoshikawa, Y., T. Yasuike, A. Yagi, and T. Yamada. 1999. Transverse elasticity of myofibrils of rabbit skeletal muscle studied by atomic force microscopy. *Biochem. Biophys. Res. Commun.* 256:13–19.